Determination of top-of-atmosphere longwave radiative fluxes: A comparison between two approaches using ScaRaB data

Ting Chen

Department of Applied Physics and Applied Mathematics, Columbia University, and NASA Goddard Institute for Space Studies, Columbia University, New York, New York, USA

William B. Rossow

NASA Goddard Institute for Space Studies, New York, New York, USA

Received 4 June 2001; revised 28 September 2001; accepted 28 September 2001; published 27 April 2002

[1] Two conceptually different approaches (broadband-based ERBE (Earth Radiation Budget Experiment) and narrowband-based ISCCP (International Satellite Cloud Climatology Project) approaches), used to derive the TOA (top of atmosphere) longwave radiative fluxes, are compared using the ScaRaB simultaneous narrowband and broadband measurements. Except for very thin cirrus clouds, differences between the ERBE and the ISCCP approaches are in general <10 W m^{-2} for the TOA LW radiative fluxes. For clear pixels the model-calculated (ISCCP approach) TOA LW radiances are systematically smaller than the observations. Compared with the radiative transfer model used in this study, the ERBE LW angular dependence models are too weakly limb darkened for optically thin clouds but too strongly limb darkened for optically thick clouds, suggesting that more accurate instantaneous TOA LW flux estimations from the ERBE approach would require additional cloud classes based on cloud height and optical thickness. *INDEX TERMS:* 3399 Meteorology and Atmospheric Dynamics: General or miscellaneous; 3359 Meteorology and Atmospheric Dynamics: Radiative processes; 3360 Meteorology and Atmospheric Dynamics: Remote sensing; *KEYWORDS:* longwave, radiation, ADM, ScaRaB, ERBE, ISCCP

1. Introduction

[2] The delicate balance between the incoming shortwave radiation and the outgoing longwave radiation at the top of the atmosphere (TOA) and its subtle regional variations is a direct indicator of the net gain/loss of radiant energy by our planet, which determines the state of the atmospheric general circulation and the climate. Since the atmospheric circulation is forced by the vertical and horizontal gradients (not the magnitudes) of radiative and latent heating/cooling, accurate knowledge of these two flux components is crucial for understanding the climate system and predicting climate change due to human activities. The TOA outgoing longwave radiation (OLR) can be directly estimated from satellite measurements of broadband radiances, such as the Nimbus-7 Earth Radiation Budget (Nimbus-7 ERB) [*Jacobowitz et al.*, 1984], the Earth Radiation Budget Experiment (ERBE) [*Barkstrom and Smith*, 1986; *Barkstrom et al.*, 1989], the Scanner for Radiation Budget (ScaRaB) [*Kandel et al.*, 1994], and the ongoing Clouds and Earth Radiant Energy System (CERES) [*Wielicki et al.*, 1996]. Alternatively, OLR can also be indirectly inferred from narrowband radiances, either by a regression-based narrowband-to-broadband conversion technique [e.g., *Ohring et al.*, 1984; *Gruber and Krueger*, 1984] or by a detailed radiative transfer calculation with the cloud and surface radiative properties retrieved from narrowband radiances (e.g., the International Satellite Cloud Climatology Project (ISCCP)) [*Schiffer and Rossow*, 1983; *Rossow and Schiffer*, 1991] and other correlative atmospheric and surface data sets as input to the radiative transfer model [e.g., *Ellingson et al.*, 1989; *Rossow and Lacis*, 1990; *Zhang et al.*, 1995; *Rossow and Zhang*, 1995; *Hatzianastassiou and Vardavas*, 1999; *Chen et al.*, 2000a, 2000b; *Chevallier et al.*, 2000]. The narrowband-to-broadband conversion technique is still used in some operational Earth Radiation Budget (ERB) products at present [e.g., *Gruber and Krueger*, 1984] despite the limitations in the single-channel narrowband-to-broadband algorithm [*Gruber et al.*, 1994]. With the advent of more accurate global observations of cloud, atmosphere, and surface properties from satellites, the approach that calculates broadband fluxes from retrieved physical quantities becomes increasingly attractive since it intrinsically separates the effects of the clouds on the radiation field from other atmospheric and surface factors so that more direct estimates of the radiative effects of clouds can be made. Moreover, the modeling approach also allows us to partition the TOA radiation budget into its surface and in-atmosphere components in a self-consistent manner [*Rossow and Lacis*, 1990].

[3] Comparison between the model-calculated OLR, using ISCCP-retrieved cloud properties and other atmospheric and surface data sets, and the ERBE OLR shows that while the two fluxes agree reasonably well in general, systematic differences exist in specific locations suggesting that particular local surface, atmospheric, and cloud conditions are responsible for the disagreement between these two products [*Rossow and Zhang*, 1995; *Xu*, 1997]. It is imperative to identify the sources of these discrepancies, because these systematic differences, though relatively small in magnitude, are certainly significant when compared with the radiation budget changes that appear interannually or that are being considered in relation to possible climate changes induced by changes in atmospheric composition (increasing abundance of greenhouse gases and aerosols) and, consequently, cannot be ignored in evaluating the effects of cloud-radiation interactions on the climate. Identifying the sources of discrepancies will also help to identify the problems associated with the two approaches. Unfortunately, examining and isolating the sources of disagreement is complicated by the effects of different temporal and spatial sampling of the ISCCP and ERBE measurements.

0148-0227/02/2001JD000914$09.00

[4] The existence of both narrowband and broadband channels on the ScaRaB radiometer provides a unique opportunity to compare the narrowband-based ISCCP and broadband-based ERBE approaches using coincident, collocated, and coangular radiance measurements and flux estimates. The narrowband channels of ScaRaB are equivalent to the visible and infrared channels used in the ISCCP cloud retrievals, while the broadband channels are similar to those of the ERBE scanners. Thus it is possible to use the ScaRaB data to retrieve the OLR using the ISCCP approach with the narrowband radiances and using the ERBE approach with the broadband radiances. Use of the ISCCP-like and ERBE-like OLRs from the ScaRaB measurements eliminates the uncertainties due to the temporal and spatial mismatches and allows us to focus on the differences between the ISCCP and the ERBE approaches, which is invaluable for the validation and improvement of both approaches and will significantly advance our understanding of ERB as a consequence. Particularly, simultaneous narrowband and broadband measurements allow us to isolate the effects of angle model differences in the analyses (the unique advantages for addressing angular model related issues provided by ScaRaB have also been exploited in the study by *Chang et al.* [2000], which focused on the TOA albedo and SW angular dependence models). Since our comparisons are restricted to the instantaneous pixel-level radiance and flux values, the differences in the space-time averaging algorithms used to obtain proper averages of the fluxes from temporally and spatially sparse samples are not considered in this study. There are other studies designed for this purpose [e.g., *Xu*, 1997]. Moreover, this particular study is only intended to identify the sources of disagreements in the ERBE and ISCCP approaches. The radiative effects of clouds using ISCCP and ERBE data are the subjects of other research efforts [e.g., *Harrison et al.*, 1990; *Hartmann and Doelling*, 1991; *Ockert-Bell and Hartmann*, 1992; *Hartmann et al.*, 1992; *Chen et al.*, 2000a, 2000b].

[5] It is worth pointing out that one of the limitations when applying the original ISCCP algorithm to ScaRaB narrowband radiances is the coarse resolution of ScaRaB. Previous studies, however, have shown that the ISCCP algorithm is rather stable with spatial resolution variations [*Briand et al.*, 1998; *Stubenrauch et al.*, 2002], which implies that this is actually a smaller problem than one might have thought. Nevertheless, considerable efforts are devoted in this study to assess and mitigate the consequence of applying the original ISCCP algorithm to the coarser ScaRaB measurements.

[6] A short description of the ScaRaB project and its ERBE-like inversion method is given in section 2. The ISCCP approach to determine OLR using the ScaRaB narrowband radiances is described in section 3. Section 4 examines the differences between the ISCCP-like and the ERBE-like OLRs as a function of ISCCP cloud parameters and discusses the possible sources of disagreements. Section 5 summarizes the main findings and discusses the implications of this study.

2. ScaRaB Project and Inversion Method

2.1. ScaRaB Project

[7] The Scanner for the Radiation Budget (ScaRaB) project is a joint project of France, Russia, and Germany intended to provide a continuation of the ERBE scanner mission [*Kandel et al.*, 1994]. The first ScaRaB flight model (FM1) was launched onboard the Russian Meteor-3/7 weather satellite with circular polar orbit at an altitude of 1200 km and an inclination of 82.5° (not Sun synchronous). The orbit plane precessed relative to the Sun-Earth vector with a period of approximately 213 days, resulting in full coverage of the diurnal cycle in about 106 days. The ScaRaB instrument is a cross-track scanning radiometer with a swath of 97.82° (that is, the maximum satellite nadir angle is 48.91°, yielding a maximum viewing zenith angle of 63.57° considering the curvature of the Earth) [*Capderou*, 1998]. The angular resolution of instantaneous field of view is 48×48 mrad^2, corresponding to a pixel size of 60×60 km^2 at nadir. The radiometer consists of two narrowband and two broadband channels with identical fields of view. The two narrowband channels are similar to the weather satellite imager channels used in the ISCCP analysis, one corresponding to the visible portion of the solar spectrum (VIS: 0.55–0.65 μm), the other to the infrared atmospheric window (IRW: 10.5–12.5 μm). The broadband shortwave (SW: 0.2–4 μm) and total radiation (TW: 0.2–50 μm) channels of ScaRaB, from which the reflected shortwave and emitted longwave radiances are derived, are analogous to those of the ERBE scanner. Daytime radiation in the longwave band (LW: nominally 4–50 μm) is obtained by appropriated weighted subtraction of the SW signal from the TW signal. The radiometric accuracy of the radiances is estimated to be better than 1% in the LW and 2% in the SW. The data were received and processed from 24 February 1994 to 6 March 1995 with some interruptions; therefore ~11 months of data have been collected [*Kandel et al.*, 1998].

2.2. Inversion Method

[8] As a follow-on of ERBE, the first version of the ScaRaB data processing was developed as an "ERBE-like version" to ensure consistency between ERBE and ScaRaB products. In other words, the ScaRaB algorithms are as close as possible to the ERBE algorithms except for some parameters used in ERBE scene identification, which are missing in the published descriptions of ERBE [*Viollier et al.*, 1995], and the steps specific to the instrument characteristics, such as the spectral corrections. (Several improvements are being planned for the future version of ScaRaB data processing, including adapting ISCCP cloud detection algotithms to the coarse spatial resolution of the ScaRaB narrowband measurements for better scene/cloud identifications and thus improved clear-sky fluxes and cloud radiative effects [*Briand et al.*, 1998; *Stubenrauch et al.*, 2002] and applying different angular dependence models from recent studies for the conversion of radiances into fluxes [e.g., *Stubenrauch et al.*, 1993].) Like all scanning radiometers, ScaRaB measures radiances at specific angles. The filtered SW and LW radiances, after radiometric calibration, are first corrected for spectral filtering effects. Spectral correction is, in general, a function of scene type. For the ScaRaB LW radiance, which is the result of weighted subtraction of the SW from the TW channels, however, the filtering error is negligible and therefore no spectral correction is applied in the current ScaRaB inversion process [*Viollier et al.*, 1995]. The ERBE angular dependence models (ADMs), which account for the anisotropy of the radiation field, are then applied to the unfiltered SW and LW radiances to obtain the SW and LW fluxes at TOA [*Suttles et al.*, 1988, 1989].

[9] Since the angular dependence models depend on the type of surface and the amount of cloud present in the observed scene, a procedure is required to identify the scene type. The algorithm of scene identification is the maximum likelihood estimation (MLE) [*Wielicki and Green*, 1989], which compares the unfiltered LW and SW radiances to a priori statistics developed from a classification of Nimbus-7 ERB data. The 12 scene classifications are the same as used by ERBE, based on a combination of five geotypes (ocean, land, snow, desert, coast) and four cloud categories: clear (0–5% cloud cover), partly cloudy (5–50% cloud cover), mostly cloudy (50–95% cloud cover), overcast (95–100% cloud cover). Very roughly, the MLE expects a clear scene to be dark and hot, cloudy scenes to be bright and cold. Presumably, the larger pixel size of ScaRaB (60 km at nadir versus 30–45 km for ERBE) should give rise to a somewhat different scene-type distribution compared with ERBE. This effect, however, is mitigated because the a priori probabilities used in the ScaRaB scene identification were computed by analyzing the scene fractions of the ERBE S-9 archive [*Viollier et al.*, 1995]. Since the objective of the ScaRaB project is

to determine the TOA ERB components on a scale appropriate to the study of cloud radiation interactions, an additional procedure is performed to obtain proper averages of the fluxes from temporally and spatially sparse samples [*Brooks et al.*, 1986]. However, as mentioned before, the problems associated with the spatial and temporal averaging algorithms are beyond the scope of this present study, since our results are restricted to the instantaneous pixel-level radiance and flux values.

[10] Similar to ERBE, three levels of ScaRaB data are produced by the data processing procedures. In particular, the second level (A2) is directly comparable to the ERBE S-8 product containing instantaneous unfiltered SW and LW radiances, estimated TOA fluxes, as well as scene identifications at the pixel level, and is the primary data source for this study [*Kandel et al.*, 1998].

3. ISCCP-Based Approach for OLR Determination

[11] The ScaRaB visible (VIS) and infrared window (IRW) channels are comparable to those used in the ISCCP analysis; thus it is a natural idea to apply the ISCCP algorithm to the ScaRaB VIS and IRW radiances. Similar to many cloud algorithms, the ISCCP algorithm consists of two basic phases: the cloud detection phase and the cloud properties derivation phase. On the basis of a series of statistical analyses of the radiance space-time variations, the cloud detection algorithm first infers the clear-sky VIS and IRW radiances for each individual pixel. An individual pixel is then classified as cloudy, if either the VIS or IRW radiance differs from its corresponding clear-sky value by more than the detection thresholds, or clear if otherwise (space/time variability test) [*Rossow and Garder*, 1993]. If the pixel is cloudy, then comparison of the observed radiances to those predicted by a radiative transfer model determines a cloud top temperature (T_c) from the IRW radiance and a visible optical thickness (τ, daytime only) from the VIS radiance. If the pixel is clear, then surface temperature (T_s) and surface visible reflectance (R_s, daytime only) are retrieved [*Rossow et al.*, 1996]. The effects of the atmosphere on the radiances are accounted for and cloud top pressure (P_c) is determined from T_c using the atmospheric temperature and humidity profile from the Television Infrared Observation Satellite (TIROS) Operational Vertical Sounder (TOVS) product [*Kidwell*, 1995]. To be consistent with the cloud and surface retrieval, the same TOVS profile is also used in the radiative transfer model calculation in this study (unless otherwise indicated).

[12] From the ScaRaB VIS and IRW radiances, cloud and surface properties are retrieved in the same form as the ISCCP DX (pixel level) data set. The ScaRaB-derived cloud and surface properties, called ScaRaB DX, are then combined with ancillary data and used as input to a radiative transfer model to calculate fluxes. The radiative transfer model is a refined version of the one described by *Zhang et al.* [1995] with similar input and output quantities. The improvements most relevant to this study are as follows: (1) The clouds are treated using an ice microphysical model if top temperature <260 K, which is consistent with the ISCCP retrieval. (2) The spectral resolution of the *k*-distribution method is increased from 25 to 33 *k*-intervals for thermal radiation [*Lacis and Oinas*, 1991]. (3) The parameterization of water continuum absorption is improved using the theoretical calculations by *Ma and Tipping* [1991, 1992a, 1992b]. (4) Nonunit emissivity is used for the surface with correction of the retrieved surface skin temperature. (5) A better interpolation for surface air temperature is introduced.

[13] For the LW radiation, which is the focus of this study, the radiative transfer model uses a three-point numerical quadrature (corresponding to emission angles of cos θ = 1.0, 0.5, and 0.1) to integrate over the angular distribution of the radiation [*Lacis and Oinas*, 1991]. A by-product of this added complexity is that we have available from the radiation model an infrared window radiance, a spectrally integrated broadband radiance (both for nadir-viewing geometry and for the more extreme emission angles of cos θ = 0.5 and 0.1), and angle-integrated fluxes. Thus the radiative transfer model can be used to simulate the narrowband and broadband ScaRaB measurements for direct comparison with the measured radiances, as well as allowing comparison of the resulting fluxes (Figure 1). This aspect of the radiative transfer model makes the ISCCP approach well suited to examine the effect that changing cloud properties have on the determination of ERB fluxes.

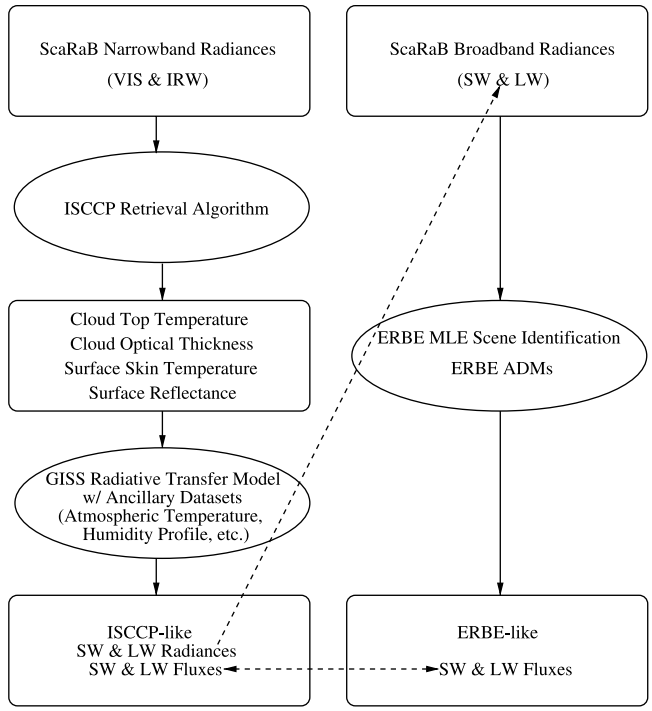

Figure 1. Schematic diagram of the basic approach used in the present study.

[14] Although all 11 months of ScaRaB FM1 narrowband radiance data have been processed through the ISCCP cloud algorithm, our analyses are performed on only 2 months of ScaRaB DX data since, typically, 1 month of ScaRaB DX data consists of several million observations and hence are enough to produce statistically significant results. However, since the satellite retrieval and flux calculation/conversion also depend on the relative geometry among Sun, Earth target, and satellite, we choose two specific months, namely May and July 1994, to provide a representative sample of Sun-target-satellite geometries. In May 1994 the daylight equator crossing time (ETC) of the satellite was around early afternoon, drifting from about 1500 local time (LT) at the beginning of the month to about 1200 LT at the end of the month. Because of the precession of the orbit, the daylight ETC changed to early morning in July 1994, varying from about 0830 at the beginning of the month to about 0700 LT in the middle of the month. Only the daytime observations are used in this study, since both approaches are more accurate for the daytime than for the nighttime observations due to the fact that lacking visible information, both the ISCCP cloud detection and the ERBE MLE scene identification algorithms degrade into single threshold tests for the nighttime observations. Besides, in the ISCCP retrieval, cloud optical thickness is determined from visible radiance measurements, which are only available during daytime, and the cloud top temperature is more accurately determined as a function of optical thickness [*Rossow et al.*, 1996; *Rossow and Schiffer*, 1999].

[15] As mentioned earlier, one of the problems encountered when applying the ISCCP algorithm to the ScaRaB measure-

Table 1. Fractions of ISCCP-Declared Scene Types Labeled "Unmixed" and "Mixed"[a]

ISCCP-Declared Scene Type	Unmixed, %	Mixed, %
Clear (893,706)	35	65
Cumulus (256,718)	42.9	57.1
Stratocumulus (330,474)	74.4	25.6
Stratus (39,940)	79.6	20.4
Altocumulus (180,303)	75.6	24.4
Altostratus (150,837)	87.9	12.1
Nimbostratus (33,238)	89.4	10.6
Cirrus (145,689)	78.4	21.6
Cirrostratus (88,668)	98.5	1.5
Deep convective (31,638)	99.5	0.5
Cloudy (1,257,505)	73.1	26.9

[a] Numbers in parentheses after each ISCCP-declared scene type denote the total number of pixels for that particular scene type (data month, May 1994).

ments arises from the coarse spatial resolution of ScaRaB measurements (60 km at nadir), since the ISCCP algorithm is optimized for use with pixel size of 4–7 km. Differences in the pixel size primarily affect the retrieval in two ways. (1) The spatial and temporal variability of the surface characteristics between different pixels decreases relative to the effect of scattered low-level cloudiness as the pixel size increases. This will cause some cloud-contaminated ScaRaB pixels to be declared clear by the original ISCCP cloud detection algorithm (due to the nature of ISCCP algorithm itself), where the thresholds in the space/time variability test are selected for use with higher spatial and temporal resolutions [*Briand et al.*, 1998; *Stubenrauch et al.*, 2002]. (2) ISCCP assumes that the cloud optical properties are uniform at pixel scales; hence the cloud cover of pixels is assumed to be either zero or 1. This assumption becomes less acceptable at the lower ScaRaB spatial resolution.

[16] To separate the clear ScaRaB DX pixels with minimal cloud contamination from the clear pixels with possible cloud contamination, the ScaRaB DX pixels are compared with the actual ISCCP DX pixels matched in both space and time as closely as possible. The comparison divides the matched ScaRaB DX pixels into two subsets, called "unmixed" and "mixed." The clear (cloudy) ScaRaB DX pixel is classified as "unmixed" only if its four nearest (within a radius of 60 km) neighboring ISCCP DX pixels are all labeled as clear (cloudy) and is classified as "mixed" otherwise. (Since the ScaRaB pixel size grows to over 200 km at 60° view, limb-viewed ScaRaB pixels should be compared with significantly more neighboring ISCCP DX pixels in theory. However, if more ISCCP DX pixels are used, the number of "unmixed" pixels decreases significantly. To retain enough "unmixed" pixels for analysis, four nearest ISCCP DX pixels are used regardless of the ScaRaB viewing angle. As a result, a portion of limb-viewing "unmixed" ScaRaB pixels are in reality "mixed." The consequences are considered in section 5.) For the "unmixed" pixels we assume that when four nearby ISCCP DX pixels are clear (cloudy), the whole region of ScaRaB DX pixels is entirely clear (cloudy). Conversely, the "mixed" pixels are more likely to be partially cloud covered. Table 1 shows the fraction of the ISCCP-declared scene types that are labeled "unmixed" or "mixed" for May 1994. On average, about 65% of the matched clear (determined by ISCCP analysis) ScaRaB DX pixels are labeled "mixed," indicating that a quite large portion of the ISCCP-declared clear ScaRaB pixels may actually contain small amount of clouds due to the lower ScaRaB spatial resolution, as pointed out by *Briand et al.* [1998]. A large majority (73%) of the ISCCP-declared cloudy ScaRaB pixels are labeled "unmixed" rather than "mixed," especially for the cloud types that are optically thick or of large size, such as deep convective or cirrostratus clouds (see Figure 2 for the ISCCP radiometric cloud classification). The only exception arises for the ScaRaB pixels determined as cumulus by the ISCCP algorithm, where more than half (57%) of them are labeled "mixed", consistent with the facts that (1) cumulus clouds tend to be of a small size and broken; and (2) partially filled cloudy pixels are more likely classified as cumulus rather than any other cloud type in the ISCCP analysis. Although completely clear or overcast does not imply that the optical properties of surface or cloud are uniform over areas of tens of kilometers, the assumption of optical homogeneity is certainly a better one for the "unmixed" pixels than for their "mixed" counterparts. It is therefore interesting to contrast the results from the "unmixed" pixels with those from the "mixed" pixels and examine to what extent the results are affected when this assumption is severely violated, as will be done in section 4.

4. Comparison Between the Two Approaches

[17] Figure 1 schematically shows the key steps involved in the present ScaRaB investigation. (1) ScaRaB narrowband radiances (VIS and IRW) are first used to retrieve the cloud and surface radiative properties using the ISCCP algorithm. The narrowband-retrieved quantities are then used as input (along with other ancillary data sets) to the radiative transfer model to calculate the broadband radiances, which will be compared with the simultaneously measured ScaRaB broadband radiances. Any discrepancies in the calculated and measured broadband radiances point to the uncertainties in the input data, satellite retrieval method, and radiative transfer model itself. (2) For the pixels where the calculated and observed radiances agree, the model-calculated fluxes are compared to the fluxes converted from the measured broadband radiances using the ERBE ADMs, as well as the ADMs parameterized by *Stubenrauch et al.* [1993 (hereinafter referred to as SDK)]. The latter ADMs use combined narrowband IRW and broadband LW observations to specifically include the effects of cloud height variations and are referred to as SDK ADMs. Thus we can isolate and examine in detail the effects of angle model differences between the two ADMs and the radiative transfer model's treatment of the angle integration and quantify the effects that clouds have on the anisotropy of the radiation field.

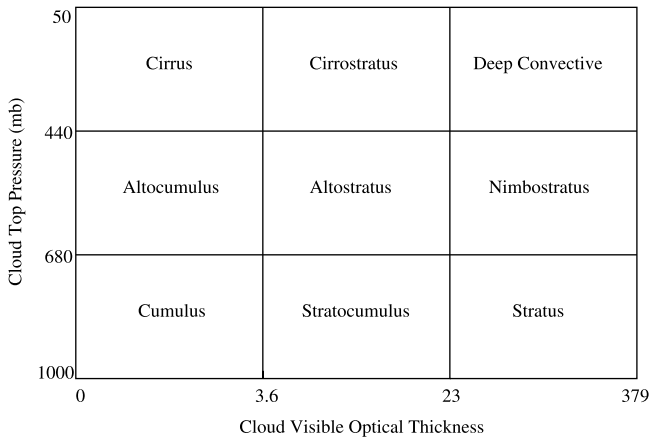

Figure 2. Definitions of the nine different cloud types by ISCCP in terms of cloud top pressure and visible optical thickness. The names used for convenience are meant to suggest qualitative relationships with the classic morphological cloud types, but they should not be interpreted to be quantitatively correct in every instance [cf. *Lau and Crane*, 1995].

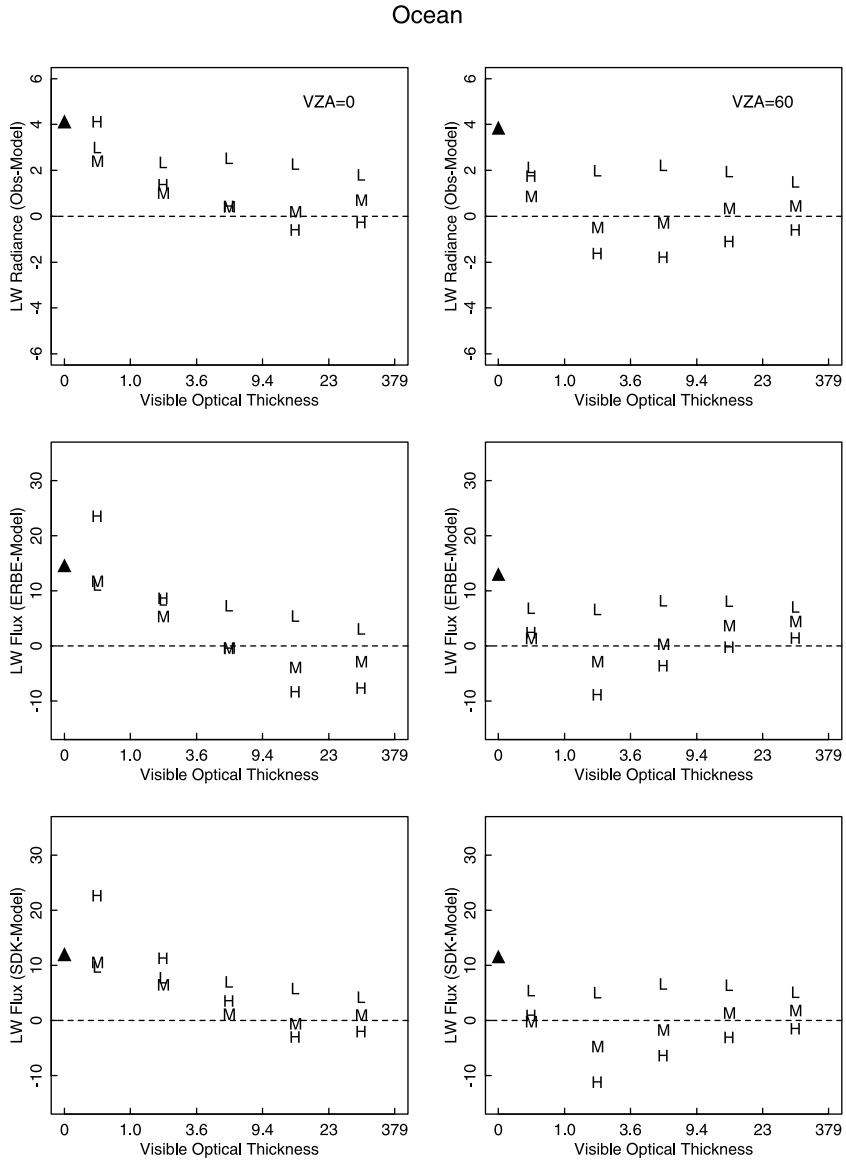

Figure 3. Mean differences (over ocean, "unmixed" pixels only) between the measured and the model-simulated TOA LW radiances (in W m^{-2} sr^{-1}), between the converted TOA LW fluxes using measured LW radiances (both of the results from ERBE ADMs and from SDK ADMs are presented) and model-calculated ones (in W m^{-2}), both for the nadir-viewing pixels (VZA = 0°) and pixels with VZA = 60°. H, M, and L denote the results for high-, middle- and low-level clouds, respectively. Triangles denote the results for clear pixels (data month, May 1994).

[18] As discussed earlier, both the ISCCP retrieval algorithm and the radiative transfer model for the flux calculation assume optical homogeneity in the underlying pixels. Undoubtedly, this assumption becomes increasingly a problem as the pixel size increases. To alleviate this problem, associated with the relatively coarse spatial resolution of ScaRaB measurements, we will first restrict the results to the "unmixed" scenes. Then the results from the "mixed" scenes will be briefly discussed to determine how the results are affected when the optical homogeneity assumptions are violated. Apart from the above mentioned optical homogeneity issue, our comparisons are complicated further by the following two differences between the ERBE and the ISCCP approaches. (1) The TOA in the ERBE analysis is chosen as 30 km (a reference altitude where latitude, longitude, and viewing geometry are defined), whereas the model calculations set TOA as 100 km (no atmosphere above 100 km). This difference in TOA definition produces a fraction of a percent difference in the LW radiances or fluxes at the TOA. (2) The synthetic ScaRaB LW channel (the result of weighted subtraction of the SW from the TW channel) has a nominal spectral range from 4 to 50 μm, whereas the model calculated LW radiance or flux represents the range from 5 to 200 μm. This difference may cause a low bias of as much as 1% in the ScaRaB LW measurements.

[19] Although we have performed the analyses on two months of ScaRaB DX data, only the results for May 1994 are shown here, since the results for July 1994 are similar.

4.1. "Unmixed" Pixels

[20] Figure 3 shows the mean differences (over ocean, "unmixed" pixels only) between the measured and the model-simulated TOA LW radiances, between the ERBE and the SDK ADM-converted and model-calculated TOA LW fluxes for May 1994. Similar results are obtained over land (not shown). Results

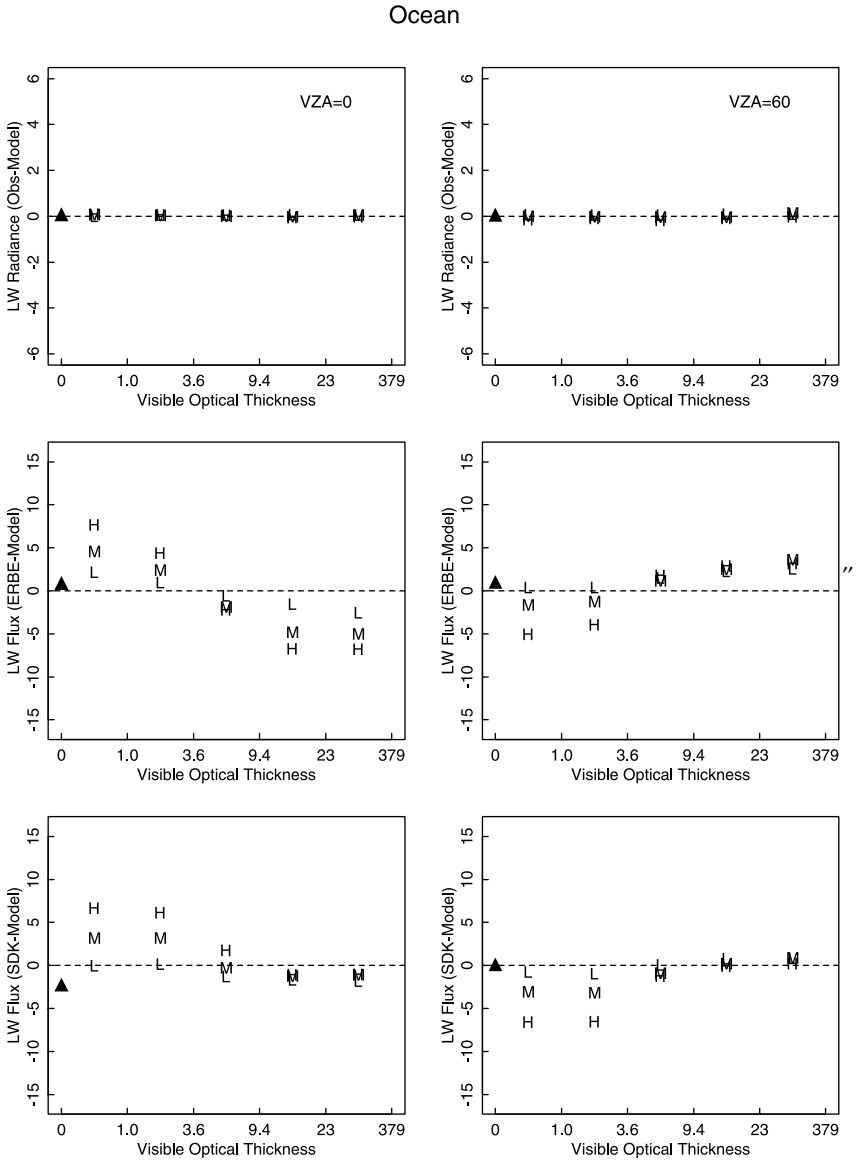

Figure 4. Same as Fig. 4, but only for the pixels where model-simulated and observed TOA LW radiances agree to within 0.5 Wm^{-2} sr^{-1} (data month, May 1994).

from clear and cloudy, from nadir- and limb-viewing pixels (VZA = 0° and 60°) are separately presented. For cloudy pixels, the differences are shown separately for low, midlevel and high clouds as a function of their optical thickness. Except for the clear and low-cloud cases, where the differences exhibit a simple latitudinal dependence (maximum in the tropics), the differences are generally independent of the geographical location, and hence only the global mean results are discussed (likewise the numbers quoted in the text, unless otherwise noted). Figure 4 is similar to Figure 3 except that only the pixels where the measured and model-simulated LW radiances agree to within 0.5 W m^{-2} sr^{-1} (overall, 29% of the available pixels meet this requirement) are included, so the LW flux difference can originate only from the difference between the ADMs used by the ERBE-like approaches and the radiative transfer model's treatment of the angle integration.

4.1.1. Clear sky and low clouds. [21] Even for the "unmixed" clear ScaRaB DX pixels, a significant portion of them (26% for May 1994 and 44% for July 1994) are identified as somewhat cloudy by the ERBE MLE method. To minimize the uncertainties in clear-sky results caused by the possible cloud contamination, only the clear "unmixed" pixels where both ISCCP and MLE agree are included in the comparison. Averaged over the globe, the clear-sky TOA LW fluxes estimated from the observed LW radiances and ERBE ADMs exceed the model calculations by more than 10 W m^{-2} for both nadir- and limb-viewing ocean pixels of May 1994 (Figure 3). Note that the flux differences shown here cannot be explained by the fact that the ERBE clear-sky TOA LW fluxes are biased high, especially in the tropics, due to the overly restrictive clear-sky definition in the ERBE analysis [cf. *Hartmann and Doelling*, 1991; *Collins and Inamdar*, 1995] for the following two reasons: (1) the current flux comparison is made on the same "unmixed" clear pixels where ISCCP and MLE agree; and (2) these "unmixed" clear pixels, by definition, tend to be found in the midst of vast regions that are clear and thus are highly unlikely to be cloud contaminated. The comparison between the observed and the model-simulated LW radiances shows that the flux differences

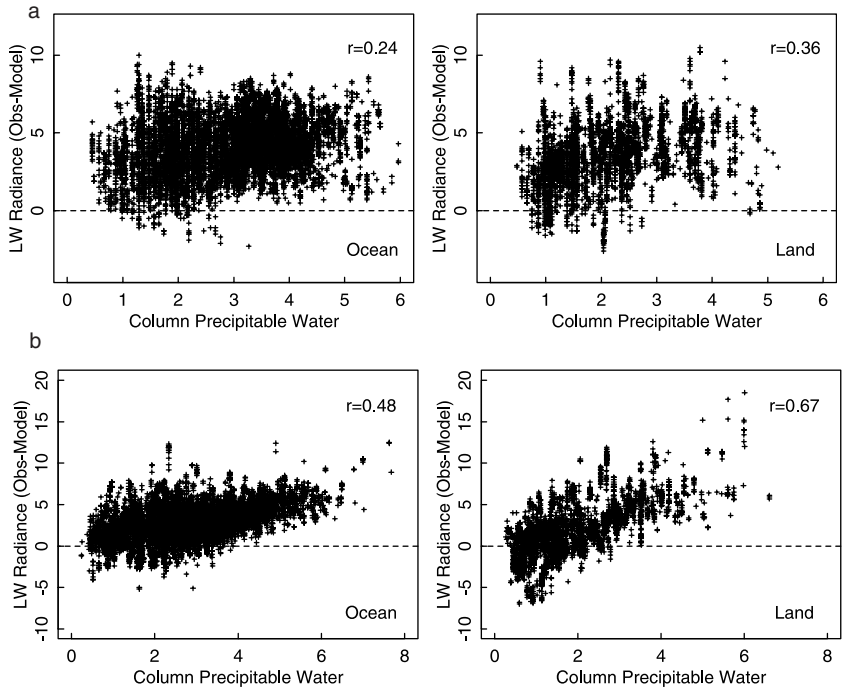

Figure 5. (a) Scatterplot of TOA LW radiance differences (in W m^{-2} sr^{-1}; observation minus calculation, nadir-viewing pixels only) against the column precipitable water using TOVS atmospheric temperature and humidity profile, along with the corresponding correlation coefficient (data month, May 1994). (b) Same as Figure 5a but for 3I atmospheric temperature and humidity profile.

largely arise from the disagreements in the broadband radiances (top panels in Figure 3).

[22] A detailed investigation of this clear-sky bias shows that there is a positive correlation between the LW radiance differences (observation minus calculation) and the total precipitable water amount (Figures 5a and 5b). Since the radiative transfer model has been verified against line-by-line calculations [cf. *Lacis and Oinas*, 1991], we suspect that the input atmospheric properties may explain this behavior. To test this, we repeated the calculations using the atmospheric profiles from the TOVS Path-finder Path-B data set (hereinafter the 3I profiles from the name of the retrieval method used [*Scott et al.*, 1999]) and the 3I profiles with the total precipitable water amount rescaled to agree with the NVAP values [*Randel et al.*, 1996]. Using the 3I profiles reduces the global mean bias in the simulated LW radiances by 1–2 W m^{-2} sr^{-1}, leading to a 3–6 W m^{-2} reduction in the global mean flux difference; however, the correlation between the LW radiance differences and the total precipitable water amount is much stronger in all months at all viewing zenith angles. Modifying the 3I humidity to agree with the NVAP values reduces the correlation somewhat primarily because of a significant reduction (increase) of water vapor (LW flux) in the subtropics. In fact, in all cases, the correlation of water vapor amounts and LW radiances is associated with the large spatial contrast between the subtropical subsidence and the tropical ascent regions. Comparing all of these humidity values with rawindsonde-based climatologies suggests that they all generally overestimate upper level humidity in the subtropics. Indeed, we can substantially reduce the global bias and the correlation by moving less than 0.5 cm of middle-level precipitable water to lower levels. This is a plausible explanation, but this result needs more study.

[23] Similar to the clear-sky results but at a reduced magnitude, both the observed LW radiances and the ADM-converted fluxes exceed the model calculations for the ScaRaB pixels, identified as containing low clouds ($P_c > 680$ mbar) by ISCCP (regardless of the MLE-derived cloud cover), due mainly to the clear-sky effect. Figure 4 shows that the TOA LW flux differences for low clouds stemming from the different angle treatments are generally very small as well, despite a weak but systematic dependence on optical thickness and viewing zenith angle.

4.1.2. High- and middle-level clouds. [24] As shown in Figure 3, for the ScaRaB pixels classified as high clouds ($P_c \leq$ 440 mbar) by ISCCP, the model-simulated LW radiances can be either less than or greater than the observed ones, depending on the optical thickness and viewing zenith angle. When the clouds are optically very thin, the model, in general, underestimates the TOA LW radiance. At nadir-viewing geometry the difference is about 4 W m^{-2} sr^{-1}. In addition to the clear-sky effect, which affects the calculated upwelling flux coming through these thin clouds, part of the bias arises from the visible adjustment procedure in the ISCCP retrieval. ISCCP first retrieves the cloud top temperature, assuming that the cloud is opaque to infrared radiation, then adjusts the retrieved cloud top temperature if the infrared transmission of the cloud estimated from the retrieved visible optical thickness is greater than 0.5%. (A small coding error in the ISCCP visible adjustment step that causes a slight overestimation of cloud top temperature and pressure for clouds with a visible optical thickness between 2 and 6 has been found. This error has been corrected for the ScaRaB DX data used in this study and for the regular ISCCP D data for 1994 and later. However, ISCCP D data for July 1983 through 1993 still contain this error (see Appendix A)). This procedure encounters difficulties with very thin clouds because the errors in the optical thickness, surface temperature, and the ratio used to relate the optical thickness value in the VIS to that in the IRW will be greatly amplified when the infrared transmission is large. Thus for the clouds with $\tau/\cos\theta < 1.2$, ISCCP tends to place them at the tropopause and reset the optical thickness to a proper value so that the infrared window (but not the VIS) radiance is preserved [*Rossow et al.*, 1996]. This treatment inevitably leads to

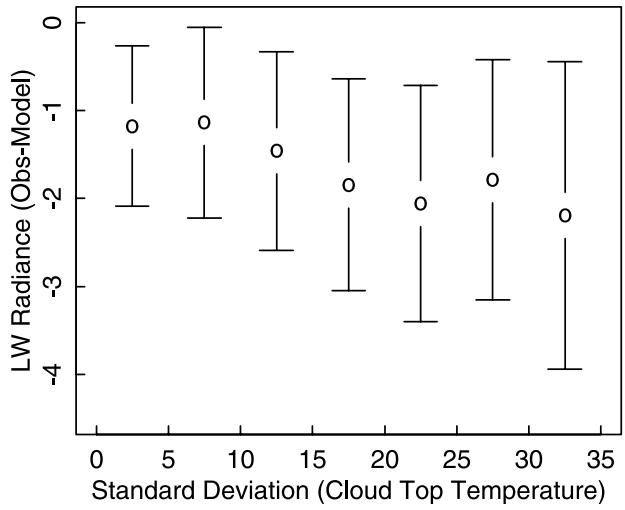

Figure 6. Mean and standard deviation of TOA LW radiance differences (in W m^{-2} sr^{-1}; observation minus calculation) as a function of σ_{Tc} (the standard deviation of cloud top temperatures over the 16 neighboring ISCCP DX pixels, in Kelvins) for the 60° view, ocean ScaRaB pixels classified as high-level clouds with optical thickness larger than 1 by ISCCP (data month, May 1994).

a cold bias in the calculated broadband longwave radiance, due to the different cloud-radiation interactions inside and outside of the infrared window wavelength range: even though the combination of T_c and τ reported by ISCCP matches the radiation in the window, if the clouds are too high, they reduce the radiation outside of the window too much.

[25] As for the high clouds with medium or large optical thickness, the model-simulated LW radiances agree rather well with the observations for nadir-viewing pixels but always exceed the observations for pixels with VZA = 60°. Noticing that the agreement is worse for the "mixed" pixels (compare Figure 7), we speculate that the larger discrepancy at 60° view is caused, at least in part, by forcing the ISCCP analysis (optimized for use with pixel size of 4–7 km) to operate on the excessively large limb-viewing pixels that tend to have a larger degree of subpixel cloud heterogeneity and brokenness (even for the "unmixed" pixels). In fact, we have repeated the analysis by comparing the ScaRaB DX pixels with the 16 nearest ISCCP DX pixels (within a radius of 200 km, roughly the size of the limb-viewing ScaRaB pixel) and found that more than half of the original "unmixed" ScaRaB DX pixels are no longer "unmixed." For those ScaRaB pixels that remain "unmixed," the standard deviation of cloud top temperatures over the 16 neighboring ISCCP DX pixels (σ_{Tc}) is computed and used as the indicator of subpixel cloud heterogeneity within each individual ScaRaB DX pixel [cf. *Stubenrauch et al.*, 1993]. We found that both the mean and the standard deviation of the discrepancy between the model-simulated and the observed LW radiances at 60° view decrease as σ_{Tc} gets smaller (Figure 6).

[26] Overall, the model-simulated radiances agree better with the measurements for the middle-level clouds (440 mbar < $P_c \leq$ 680 mbar). However, this agreement is more likely due to the cancellation of two opposing effects, namely the "clear-sky" bias and "subpixel cloud heterogeneity/brokenness" effects, with both effects operating at a smaller magnitude. As a result, the vertical distribution of the longwave cooling and surface radiation might not be correctly simulated, even if the TOA radiation is correctly calculated for the midlevel clouds.

4.1.3. ERBE and SDK ADMs and the model's treatment of angle integration. [27] The fact that the differences in ADM-converted and model-calculated flux only approximately follow the radiance differences suggests that part of the flux differences are caused by the difference between the ADMs used and the radiative transfer model's treatment of angle integration. Although the relative contribution of the different angle treatments to the flux differences is difficult to determine exactly, Figure 4 does provide some insight.

[28] We first consider the ERBE ADMs. It is observed in Figure 4 that for the nadir view, when the observed and the model-simulated radiances agree, the ERBE ADM-converted fluxes are higher (lower) than the model-calculated ones for clouds with small (large) optical thickness, regardless of the cloud height. The opposite is true for the 60° view. This indicates that compared with the radiative transfer model, the limb darkening in the ERBE angular models is too weak for the optically thin clouds ($\tau < 3.6$) but too strong for the optically thick clouds ($\tau > 9.4$). When all clouds are averaged together, however, the limb darkening in the ERBE angular models closely resemble that implied by the radiative transfer model (not shown). From first principles, for clouds at the same height, optically thin clouds should be more limb darkened than the optically thick clouds. For instance, Because of the sec θ dependence of radiation path length through the cloud layer, optically thin cirrus can be nearly transparent to LW radiation at near-nadir viewing angles, while the same cloud can be nearly opaque to LW radiation at near-limb-viewing angles, leading to the limb darkening even stronger than that for clear-sky conditions [*Wielicki and Green*, 1989]. On the other hand, optically thick clouds are usually more Lambertian than clear scenes. These results suggest that the ERBE ADMs represent the anisotropy of the LW radiation averaged over all cloud types but not for particular cloud types. This is not surprising, considering that the ERBE ADMs are based on a large set of Nimbus-7 ERB observations without explicit distinction of different cloud optical properties. As pointed out by *Stubenrauch et al.* [1993], if the dependence of angular models on the cloud properties was not taken into account in their construction, it must be averaged out in the final products. In fact, this is exactly what happened, since the longwave ERBE ADMs are all quite similar with angle variations of only 1–2%, on average, among the four cloud cover conditions [*Suttles et al.*, 1989]. Also notice in Figure 4 that the difference between the ERBE ADMs and the angle treatment of the radiative transfer model increases with cloud height. As a result, the differences in the estimated fluxes caused by the different angle treatments between the ERBE and the ISCCP approaches are not the same for the low as for the high clouds. This is very important since the radiative flux gradient, one of the ultimate forcings driving the atmospheric circulation, between the climate regimes characterized by persistent but different cloud types is not equally represented by these two approaches. Yet this difference in the gradient cannot be completely eliminated in the final space- and time-averaged products, as will be discussed in section 4.2.

[29] Figure 4 shows that for the optically thick clouds ($\tau > 9.4$) the SDK ADMs and the radiative transfer model's angle treatment are very similar. This is anticipated since the SDK ADMs are developed on the basis of radiative transfer calculations assuming a horizontally homogeneous surface or cloud layer of unit emissivity [*Stubenrauch et al.*, 1993]. Interestingly, for the optically thin clouds the SDK ADMs appear to behave more like the ERBE ADMs, but this result may vary, depending on how the optically thin clouds are defined by different methods [cf. *Stubenrauch et al.*, 1993].

4.2. "Mixed" Pixels

[30] Figures 7 and 8 are the same as Figures 3 and 4, respectively, except they show results for the "mixed" pixels.

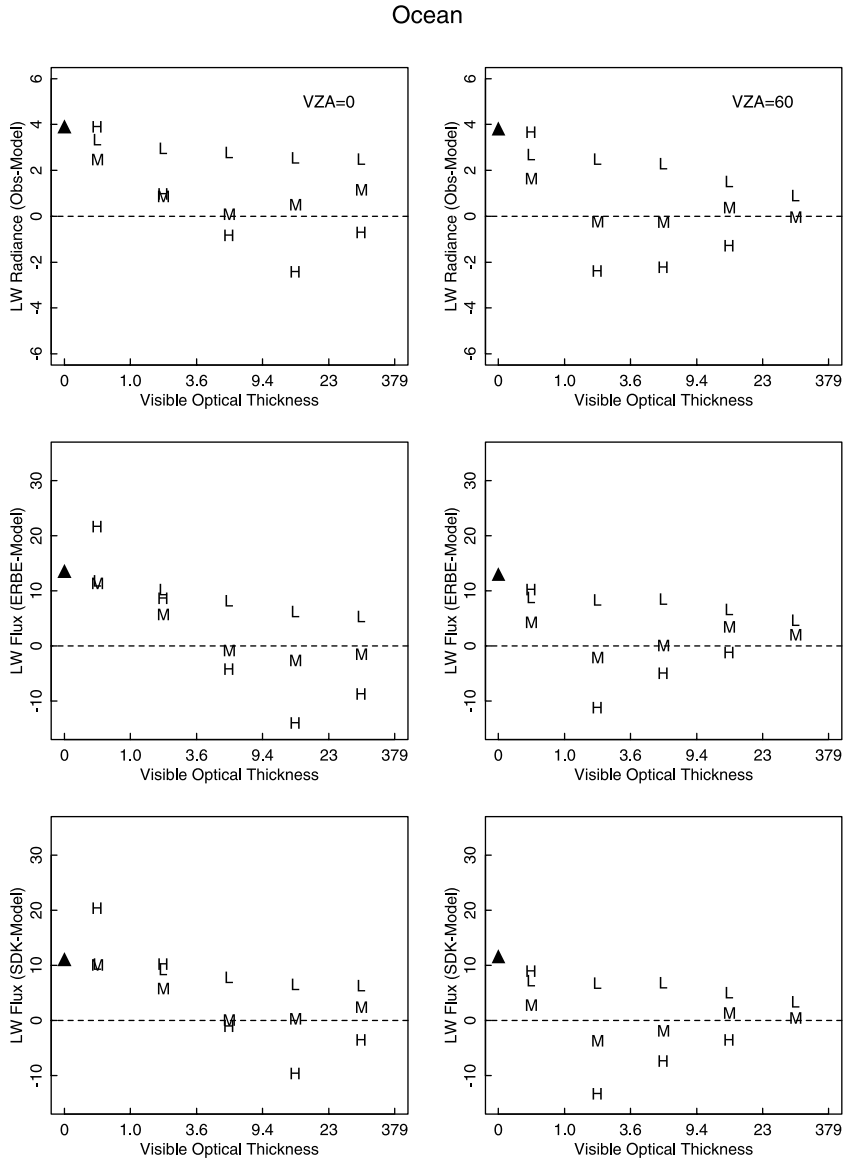

Figure 7. Same as Figure 3 but for the "mixed" pixels only.

For high-level broken cloud fields, the agreement between model-simulated and observed LW radiances deteriorates. However, this effect is rather small on the global scale, considering the relatively infrequent occurrence of high-level broken cloudiness. The majority of the broken cloudiness is confined to the low-level small cumulus clouds in the trade wind regimes. For middle- and low-level clouds, the patterns shown in Figure 7 are very similar to those in Figure 3, indicating that the uncertainties in the estimated TOA longwave radiation budget caused by broken cloudiness are quite small, even at the coarse spatial resolution of ScaRaB. This can be explained by the cancellation of two offsetting effects. In the presence of broken cloudiness the radiance used to retrieve the cloud is an averaged value from the actual clouds and surface; hence the retrieved cloud assumed to cover the entire pixel is, on average, lower and optically thinner than the actual clouds. The larger cloud cover tends to decrease the longwave radiation, whereas the higher cloud top temperature and smaller optical thickness tend to increase the longwave radiation. In the low-cloud cases the effect of broken cloudiness on the TOA longwave radiation budget is even smaller because the TOA longwave radiation is largely determined by the atmosphere above the clouds.

5. Summary and Discussion

[31] Two conceptually different approaches (broadband-based ERBE and narrowband-based ISCCP approaches), used to derive the TOA longwave radiative fluxes, are compared using the ScaRaB simultaneous narrowband and broadband measurements (compare Figure 1). For the clear sky the model underestimates the observed TOA LW radiances on the global average with the bias correlated to the column precipitable water amount. Although this bias can be substantially reduced by changing the water vapor profiles at lower latitudes, the exact source of the bias still requires study. A similar but smaller bias is also observed for the low clouds, primarily due to the clear-sky effect since the TOA longwave radiation is largely determined by the atmosphere above when the clouds are low level. For high

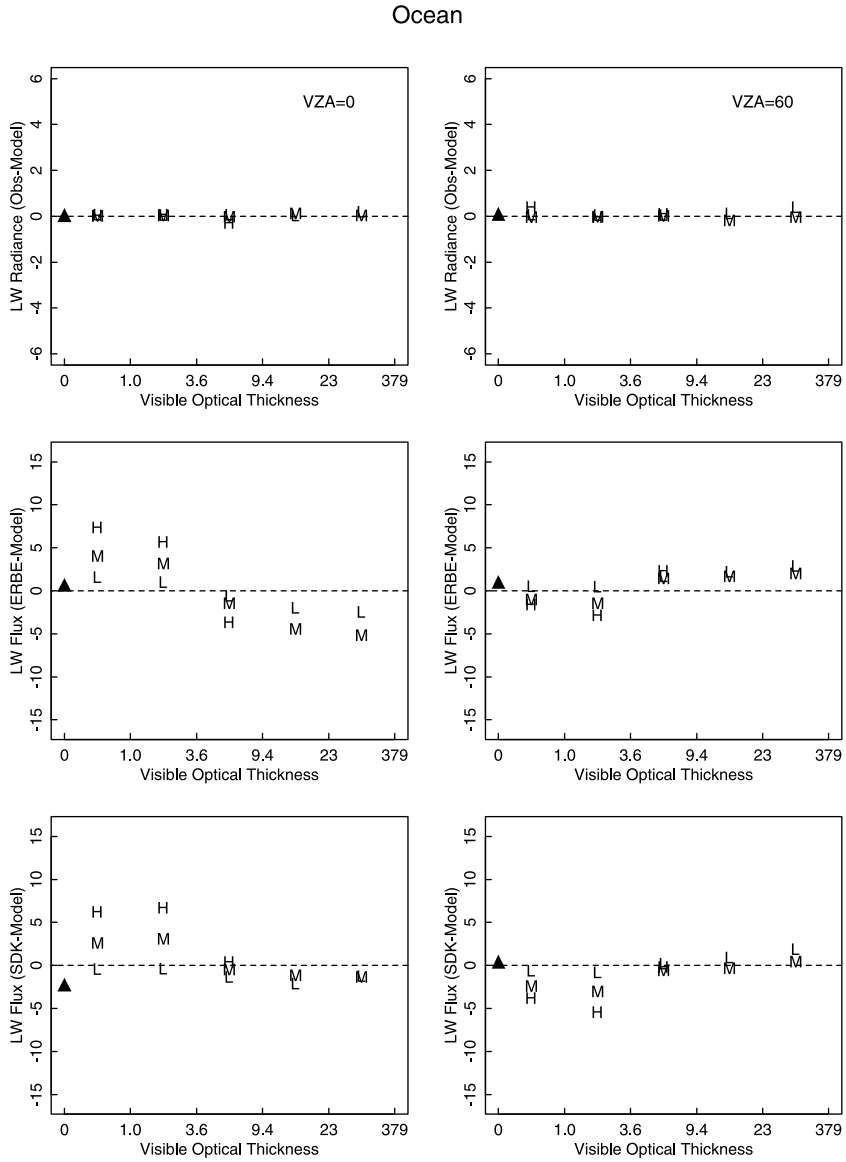

Figure 8. Same as Figure 4 but for the "mixed" pixels only.

clouds, depending on the optical thickness, the model-simulated LW radiances can be either less than or greater than the observed ones. When the clouds are optically very thin, the model underestimates the TOA LW radiance partly as a result of the fact that these clouds tend to be placed too high during the visible adjustment step of the ISCCP retrieval. In general, the modeled TOA LW radiances agree better with observations for the nadir-viewing pixels than for the pixels viewed from limb, since the excessively large limb-viewing pixels are more likely to be heterogeneous or partially cloud filled.

[32] Compared with the radiative transfer model, the limb darkening in the ERBE angular models appears to be too weak for the optically thin clouds but too strong for the optically thick clouds, and the difference between the ERBE ADMs and the angle treatment of the radiative transfer model increases with cloud height. Limitations in the radiative transfer model calculations, however, prevent definitive judgment on the ERBE angular models for the following reasons: (1) The radiative transfer model's angle treatment is sensitive to the uncertainties in the cloud vertical structure (e.g., multilayer clouds); and (2) the ERBE ADMs are generated using the complete range of observed cloud conditions, not just clear and overcast, whereas the plane-parallel radiative transfer model used in this study inevitably assumes optical homogeneity on the underlying pixels, which tends to underestimate the limb darkening for the broken three-dimensional cloud fields. Nevertheless, this study clearly demonstrates that obtaining more accurate instantaneous longwave flux estimations from the ERBE approach would require additional cloud classes based on cloud height and optical thickness as is planned for the advanced CERES analysis [*Wielicki et al.*, 1996].

[33] One of the rationales behind the ERBE approach is that the viewing zenith angle dependence of derived longwave flux caused by errors in the angular models will be significantly reduced in the final space- and time-averaged fluxes. This error reduction results from the fact that the ERBE angular models are normalized by the hemispherical flux based on the integral relationship between radiance and flux [*Suttles et al.*, 1989]. Over a long enough time period, a satellite will view a given region of the Earth from a wide range of viewing zenith angles,

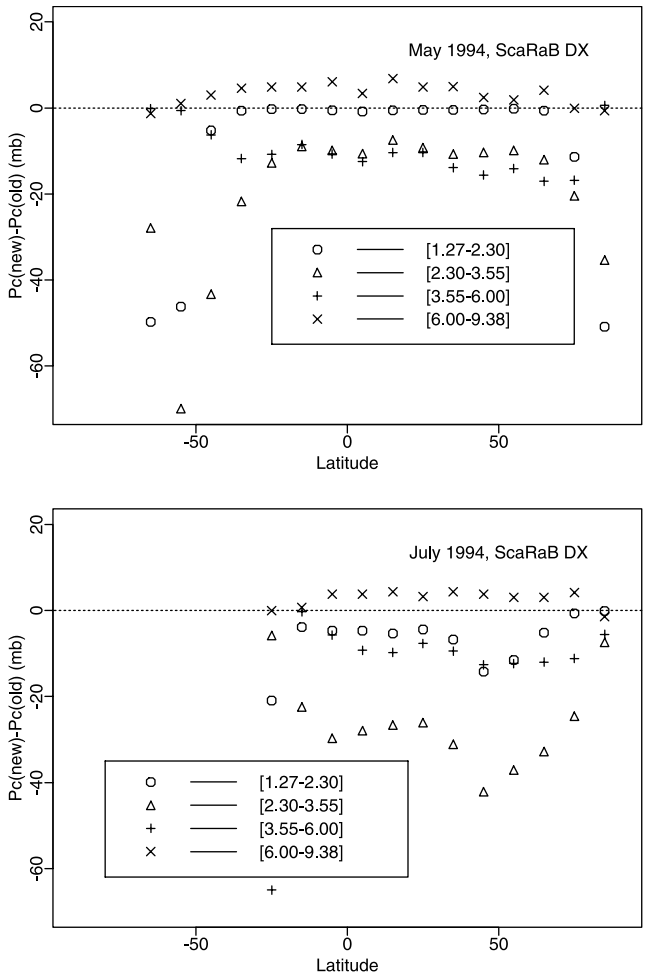

Figure A1. Zonal mean difference between the ScaRaB DX cloud top pressure retrieved using the revised ISCCP cloud program and the program with a coding error in the visible adjustment step for May and July 1994. Results from four different optical thickness intervals are presented separately.

in effect averaging over the viewing zenith angle dependence of the derived longwave fluxes. However, the errors cannot be completely eliminated (1) because of the inability of a satellite platform to provide a uniform sampling in angle [*Suttles et al.*, 1992] and (2) because a particular radiometer may only scan over a limited range of viewing zenith angles (for example, the maximum viewing zenith angle of ScaRaB scanning radiometer is 63.57°) or the measurements are not used beyond a cutoff nadir angle since the measurements become increasingly difficult to interpret in terms of the radiant exitance [*Smith et al.*, 1986]. Together with the fact that the magnitudes of the errors are cloud-type dependent, these residual errors will certainly introduce systematic regional errors in the estimated mean and temporal variations of the TOA LW radiation field. For example, as one of the better known interannual variations in climate, the El Niño-Southern Oscillation (ENSO) is characterized by large changes in cloud types in consequence of changes in the general circulation pattern in the tropical atmosphere. Unless these systematic cloud-type-dependent errors are eliminated, one cannot accurately quantify the spatial and temporal variations in the TOA LW radiative fluxes associated with an ENSO event. Likewise, the ERBE-estimated TOA LW radiative flux gradient across the equatorial Pacific Ocean needs to be revisited, considering the persistent and pronounced differences in cloud types over the ascending and descending branches of Walker circulation.

Appendix A: Error in the Visible Adjustment Step of the ISCCP Cloud Retrieval

[34] For each cloudy pixel, ISCCP first retrieves the cloud top temperature, assuming that the cloud is opaque to infrared radiation, then adjusts the retrieved cloud top temperature and visible optical thickness through iteration if the infrared transmission of the cloud is greater than 0.5% [*Rossow et al.*, 1996]. Unfortunately, a small coding error in the ISCCP cloud retrieval program, which occasionally causes this iteration to stop prematurely, has been found (for the May 1994 ScaRaB DX, this coding error affects about 13% of daytime cloudy pixels). Even though the retrieval program was modified to rectify this error to produce the ScaRaB DX used in this study (as well as for the regular ISCCP data product beyond 1993), we document the error and assess to what extent it affects the retrieved cloud properties and calculated TOA radiative fluxes.

[35] Figure A1 shows the zonal mean difference between the ScaRaB DX cloud top pressure retrieved using the revised program and the program with the coding error in the visible adjustment step. By presenting the results from different optical thickness intervals separately, it is clear that this error is most noticeable for the cloudy pixels with medium optical thickness values (approximately from 2 to 6) and usually gives rise to a cloud top temperature/pressure value that is a bit too large (about 60 mbar in P_c in the worst case). Similar results were also obtained for 1-month (July 1994) NOAA DX data (not shown). It is also observed that this error decreases as cloud top temperature/pressure increases (not shown). Correction of this error has the effect of moving the cloudy pixels a little bit higher in altitude while also making them slightly optically thinner, resulting in only a very small shift in the relative abundance of the standard ISCCP cloud types. Analysis shows that the small shift occurs mostly from altostratus to cirrus clouds with the changes in either cloud-type amounting to less than 1% (absolute value).

[36] Figure A2 examines the resulting difference in the model-calculated TOA LW radiative fluxes using 1-month (May 1994) ScaRaB DX data (revised minus flawed). This figure shows that

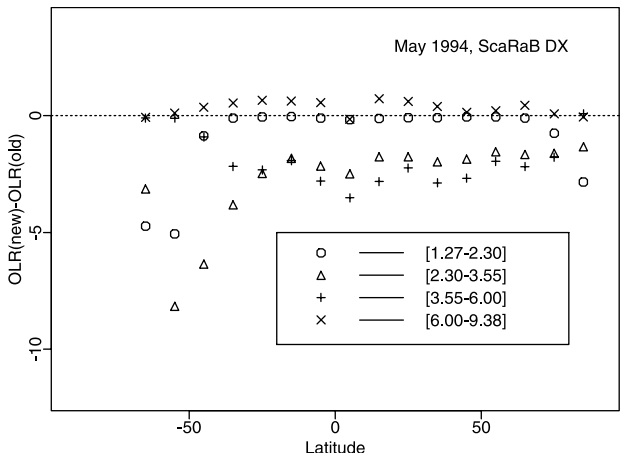

Figure A2. Zonal mean difference in the model-calculated TOA LW radiative fluxes (in W m^{-2}) using May 1994 ScaRaB DX data (revised minus flawed).

the error leads to an overestimation of several W m^{-2} in the zonal mean TOA LW fluxes for clouds with medium optical thickness values, consistent with the bias in the retrieved cloud top pressure. When all pixels (cloudy and clear) are included, the global mean TOA LW flux bias owing to this error is only 0.6 W m^{-2}, indicating that the overall impact of this error on the TOA radiation budget calculation is quite small.

[37] **Acknowledgments.** We are grateful to Claudia J. Stubenrauch for very stimulating discussions and Yuanchong Zhang for his assistance with the radiative transfer model and for preparing various data sets. This work is supported by the NASA Radiation Sciences Program, previously managed by Robert Curran and now by Donald Anderson.

References

Barkstrom, B. R., and G. L. Smith, The Earth Radiation Budget Experiment: Science and implementation, *Rev. Geophys.*, *24*, 379–390, 1986.

Barkstrom, B. R., E. F. Harrison, G. L. Smith, R. N. Green, J. Kibler, and R. Cess, Earth Radiation Budget Experiment (ERBE) archival and April 1985 results, *Bull. Am. Meteorol. Soc.*, *70*, 1254–1262, 1989.

Briand, V., C. J. Stubenrauch, W. B. Rossow, A. Walker, and R. Holz, Scene identification for ScaRaB data: The ISCCP approach, in *Satellite Remote Sensing of Clouds and the Atmosphere*, edited by J. D. Haigh, pp. 242–252, Int. Soc. for Opt. Eng., Bellingham, Wash., 1998.

Brooks, D. R., E. H. Harrison, P. Minnis, J. T. Suttles, and R. Kandel, Development of algorithms for understanding the temporal and spatial variability of the Earth's Radiation Balance, *Rev. Geophys.*, *24*, 422–438, 1986.

Capderou, M., Confirmation of helmholtz reciprocity using ScaRaB satellite data, *Remote Sens. Environ.*, *64*, 266–285, 1998.

Chang, F.-L., Z. Li, and A. P. Trishchenko, The dependence of TOA reflectance anisotropy on cloud properties inferred from ScaRaB satellite data, *J. Appl. Meteorol.*, *39*, 2480–2493, 2000.

Chen, T., W. B. Rossow, and Y.-C. Zhang, Radiative effects of cloud-type variations, *J. Clim.*, *13*, 264–286, 2000a.

Chen, T., Y.-C. Zhang, and W. B. Rossow, Sensitivity of atmospheric radiative heating rate profiles to variations of cloud layer overlap, *J. Clim.*, *13*, 2941–2959, 2000b.

Chevallier, F., F. Chéruy, R. Armante, C. J. Stubenrauch, and N. A. Scott, Retrieving the clear-sky vertical longwave radiative budget from TOVS: Comparison of a neural network-based retrieval and a method using geophysical parameters, *J. Appl. Meteorol.*, *39*, 1527–1543, 2000.

Collins, W. D., and A. K. Inamdar, Validation of clear-sky fluxes for tropical oceans from the Earth Radiation Budget Experiment, *J. Clim.*, *8*, 569–578, 1995.

Ellingson, R. G., D. Yanuk, H. T. Lee, and A. Gruber, A technique for estimating outgoing longwave radiation from HIRS radiance observations, *J. Atmos. Oceanic Technol.*, *6*, 706–711, 1989.

Gruber, A., and A. F. Krueger, The status of the NOAA outgoing longwave radiation data set, *Bull. Am. Meteorol. Soc.*, *65*, 958–962, 1984.

Gruber, A., R. Ellingson, P. Ardanuy, M. Weiss, S. K. Yang, and S. N. Oh, A comparison of ERBE and AVHRR longwave flux estimates, *Bull. Am. Meteorol. Soc.*, *75*, 2115–2130, 1994.

Harrison, E. F., P. Minnis, B. R. Barkstrom, V. Ramanathan, R. D. Cess, and G. G. Gibson, Seasonal variation of cloud radiative forcing derived from the Earth Radiation Budget Experiment, *J. Geophys. Res.*, *95*, 18,687–18,703, 1990.

Hartmann, D. L., and D. Doelling, On the net radiative effectiveness of clouds, *J. Geophys. Res.*, *96*, 869–891, 1991.

Hartmann, D. L., M. E. Ockert-Bell, and M. L. Michelsen, The effect of cloud type on Earth's energy balance: Global analysis, *J. Clim.*, *5*, 1281–1304, 1992.

Hatzianastassiou, N., and I. Vardavas, The net radiation budget of the Northern Hemisphere, *J. Geophys. Res.*, *104*, 27,341–27,359, 1999.

Jacobowitz, H., H. V. Soule, H. L. Kyle, F. B. House, and the Nimbus 7 ERB Experiment Team, The Earth Radiation Budget (ERB) experiment: An overview, *J. Geophys. Res.*, *89*, 5021–5038, 1984.

Kandel, R. S., J.-L. Monge, M. Viollier, L. A. Pakhomov, V. I. Adasko, R. G. Reitenbach, E. Raschke, R. Stuhlmann, The ScaRaB project: Earth radiation budget observations from the Meteor satellites, World Space Congress (Washington 1992)_COSPAR Symp. A.2-S., *Adv. Space Res.*, *14*(1), 47–54, 1994.

Kandel, R., M. Viollier, P. Raberanto, J. P. Duvel, L. A. Pakhomov, V. A. Golovko, A. P. Trishchenko, J. Mueller, E. Raschke, and R. Stuhlmann, and the International ScaRaB Scientific Working Group (ISSWG), The ScaRaB earth radiation budget data set, *Bull. Am. Meteorol. Soc.*, *79*, 765–783, 1998.

Kidwell, K. B., *NOAA Polar Orbiter Data Users Guide* (TIROS-N, NOAA-6, NOAA-7, NOAA-8, NOAA-9, NOAA-10, NOAA-11, NOAA-12, NOAA-13 and NOAA-14), 394 pp., Natl. Environ. Satell., Data and Inf. Service, Washington, D. C., 1995.

Lacis, A. A., and V. Oinas, A description of the correlated *k*-distribution method for modeling nongrey gaseous absorption, thermal emission, and multiple scattering on vertically inhomogeneous atmospheres, *J. Geophys. Res.*, *96*, 9027–9063, 1991.

Lau, N.-C., and M. W. Crane, A satellite view of the synoptic-scale organization of cloud properties in midlatitude and tropical circulation systems, *Mon. Weather Rev.*, *123*, 1984–2006, 1995.

Ma, Q., and R. H. Tipping, A far wing line shape theory and its application to the water vapor continuum absorption in the infrared region, I, *J. Chem. Phys.*, *95*, 6290–6301, 1991.

Ma, Q., and R. H. Tipping, A far wing line shape theory and its application to the water vibrational bands, II, *J. Chem. Phys.*, *96*, 8655–8663, 1992a.

Ma, Q., and R. H. Tipping, A far wing line shape theory and its application to the foreign-broadened water continuum absorption, III, *J. Chem. Phys.*, *97*, 818–828, 1992b.

Ockert-Bell, M. E., and D. L. Hartmann, The effect of cloud type on earth's energy balance: Results for selected regions, *J. Clim.*, *5*, 1158–1171, 1992.

Ohring, G., A. Gruber, and R. Ellingson, Satellite determinations of the relationship between total longwave radiation flux and infrared window radiance, *J. Clim. Appl. Meteorol.*, *23*, 416–425, 1984.

Randel, D. L., T. H. Vonder Haar, M. A. Ringerud, G. L. Stephens, T. J. Greenwald, and C. L. Combs, A new global water vapor data set, *Bull. Am. Meteorol. Soc.*, *77*, 1233–1246, 1996.

Rossow, W. B., and L. C. Garder, Cloud detection using satellite measurements of infrared and visible radiances for ISCCP, *J. Clim.*, *6*, 2341–2369, 1993.

Rossow, W. B., and A. A. Lacis, Global, seasonal cloud variations from satellite radiance measurements, part II, Cloud properties and radiative effects, *J. Clim.*, *3*, 1204–1253, 1990.

Rossow, W. B., and R. A. Schiffer, ISCCP cloud data products, *Bull. Am.. Meteorol. Soc.*, *72*, 2–20, 1991.

Rossow, W. B., and R. A. Schiffer, Advances in understanding clouds from ISCCP, *Bull. Am. Meteorol. Soc.*, *80*, 2261–2288, 1999.

Rossow, W. B., and Y.-C. Zhang, Calculation of surface and top of atmosphere radiative fluxes from physical quantities based on ISCCP data sets, 2, Validation and first results, *J. Geophys. Res.*, *100*, 1167–1197, 1995.

Rossow, W. B., A. W. Walker, D. E. Beuschel, and M. D. Roiter, International Satellite Cloud Climatology Project (ISCCP) documentation of new cloud data sets, *Tech. Doc. WMO/TD 737*, 115 pp., World Clim. Res. Programme, Geneva, Switzerland, 1996.

Schiffer, R. A., and W. B. Rossow, The International Satellite Cloud Climatology Project (ISCCP): The first project of the World Climate Research Program, *Bull. Am. Meteorol. Soc.*, *64*, 779–784, 1983.

Scott, N. A., A. Chédin, R. Armante, J. Francis, C. Stubenrauch, J.-P. Chaboureau, F. Chevallier, C. Claud, and F. Chéruy, Characteristics of the TOVS Pathfinder Path-B Dataset, *Bull. Am. Meteorol. Soc.*, *80*, 2679–2702, 1999.

Smith, G. L., R. N. Green, E. Raschke, L. M. Avis, J. T. Suttles, B. A. Wielicki, and R. Davies, Inversion methods for satellite studies of the earth's radiation budget: Development of algorithms for the ERBE mission, *Rev. Geophys.*, *24*, 407–421, 1986.

Stubenrauch, C., J.-P. Duvel, and R. S. Kandel, Determination of longwave anisotropic emission factors from combined broad- and narrowband radiance measurements, *J. Appl. Meteorol.*, *32*, 848–856, 1993.

Stubenrauch, C., V. Briand, and W. B. Rossow, The role of clear sky identification in the study of cloud radiative effects: Combined analysis from ISCCP and the Scanner of Radiation Budget (ScaRaB), *J. Appl. Meteorol.*, *41*, 396–412, 2002.

Suttles, J. T., R. N. Green, P. Minnis, G. L. Smith, W. F. Staylor, B. A. Wielicki, I. J. Walker, D. F. Young, V. R. Taylor, and L. L. Stowe, *Angular Radiation Models for Earth-Atmosphere System*, vol. 1, *Shortwave Radiation*, *NASA Ref. Publ. RP 1184*, vol. I, 144 pp., Langley Res. Cent., Hampton, Va., 1988.

Suttles, J. T., R. N. Green, G. L. Smith, B. A. Wielicki, I. J. Walker, V. R. Taylor, and L. L. Stowe, *Angular Radiation Models for Earth-Atmosphere System,* vol. II, *Longwave Radiation*, *NASA Ref. Publ. RP 1184*, vol. II, 84 pp., Langley Res. Cent., Hampton, Va., 1989.

Suttles, J. T., B. A. Wielicki, and S. Vemury, Top-of-atmosphere radiative fluxes: Validation of ERBE scanner inversion algorithm using *Nimbus-7* ERB data, *J. Appl. Meteorol.*, *31*, 784–796, 1992.

Viollier, M., R. Kandel, and P. Raberanto, Inversion and space-time-averaging algorithms for ScaRaB (Scanner for the Earth Radiation Budget)—Comparison with ERBE, *Ann. Geophys.*, *13*, 959–968, 1995.

Wielicki, B. A., and R. N. Green, Cloud identification for ERBE radiative flux retrieval, *J. Appl. Meteorol.*, *28*, 1133–1146, 1989.

Wielicki, B. A., B. R. Barkstrom, E. F. Harrison, R. B. Lee III, G. L. Smith, and J. E. Cooper, Clouds and the Earth's Radiant Energy System (CERES): An Earth Observing System Experiment, *Bull. Am. Meteorol. Soc.*, *77*, 853–868, 1996.

Xu, F., Outgoing longwave radiation (OLR): Variability and retrieval, 173 pp., Ph.D. dissertation, Columbia Univ., New York, N. Y., 1997.

Zhang, Y.-C., W. B. Rossow, and A. A. Lacis, Calculation of the surface and top of atmosphere radiative fluxes from physical quantities based on ISCCP data set, 1, Method and sensitivity to input data uncertainties, *J. Geophys. Res.*, *100*, 1149–1165, 1995.

T. Chen and W. B. Rossow, NASA Goddard Institute for Space Studies, Columbia University, 2880 Broadway, New York, NY 10025, USA. (tchen@giss.nasa.gov)